ChemComm

Accepted Manuscript

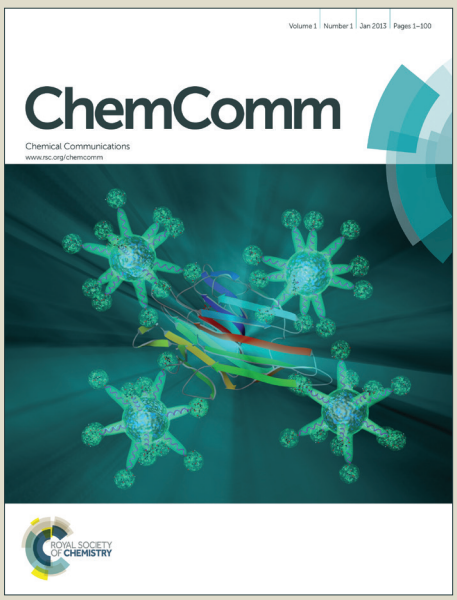

ROYAL SOCIETY OF CHEMISTRY

www.rsc.org/chemcomm

Porous inorganic nanostructures with colloidal dimensions: Synthesis and applications in electrochemical energy devices.

Pedro Tartaj,* Jose M. Amarilla

Instituto de Ciencia de Materiales de Madrid (CSIC), Campus Universitario de Cantoblanco, 28049, Madrid, Spain

*e-mail: ptartaj@icmm.csic.es

Abstract. Porous inorganic nanostructures with colloidal dimensions can be considered as ideal components of electrochemical devices that operate on renewable energy sources. They combine nanoscale properties with good accessibility, high number of active sites, short diffusion distances and good processability. Herein, we review some of the liquid-phase routes that lead to the controlled synthesis of these nanostructures in the form of non-hollow, hollow or yolk-shell configurations. From solar and fuel cells to batteries and supercapacitors, we put special emphasis on showing how these sophisticated structures can enhance the efficiency of electrochemical energy devices.

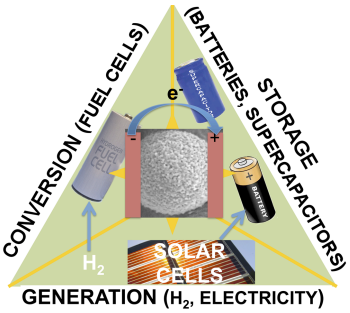

1. Introduction

Movement is essential for human development, and fossil fuels have been in charge of feeding this movement since the industrial revolution. However, both shortage and environmental risks (say for example greenhouse gas emissions) demand for alternative energy sources that in the ideal scenario must approach the landmark of being renewable. An energy source can be considered renewable when comes from resources that are in continuous replenishment on a human timescale.[1] Solar, wind, rain, geothermal heat, tides, or waves are examples of renewable energy sources. Of course, these sources must be complemented with clean and efficient technologies to minimize environmental impact. Movement implemented by renewable energy sources and clean and efficient processes is, thus, fundamental for a sustainable development (i.e. to provide conditions for long time preservation within the human timescale perception).

From generation to conversion and storage, devices that operate on electrochemical principles are considered a well-established technology for a clean handling of renewable energy sources.[2] Thus, devices in which solar energy is coupled with electrochemical reactions are perhaps the friendliest to generate molecular hydrogen from water splitting.[3] Fuel cells are also considered a well-established technology for a clean conversion of the chemical energy stored in a fuel (hydrogen) into electricity.[4] Clean electricity can also be produced using electrochemical photovoltaic devices such as dye-sensitized solar cells (Gratzel cells).[5] Furthermore, when electricity is produced there is a need to be delivered almost at the rate of its generation. As renewable energies do no meet the criteria of production on demand, storage is needed. Electrochemical devices such as batteries represent nowadays a good alternative to store and deliver electricity on demand.[6] Electrochemical capacitors (supercapacitors) are also electrochemical devices that are gaining interest because of their highly reversible capacity to store/deliver energy in a short period of time.[7] When compared to batteries they have higher power density but lower energy density. Therefore, they are intended to cover a segment between that of traditional capacitors and batteries.[8]

Indeed renewable energy sources coupled with electrochemical reactions represent a clean alternative to fossil fuels. Efficiency, however, must be significantly increased to approach fossil fuels performance. Broad consensus exists that inorganic materials with sizes within the nanoscale must be used at some extent in order to increase such efficiency.[8-11] At the nanoscale the distances are shortened, whereby favoring for example redox reactions in batteries,[12] and charge migration without recombination processes in water splitting applications.[13] Band-gap engineering is also possible at the nanoscale in

photoelectrochemical cells as light-absorption processes can be tuned changing size and shape.[14,15] Furthermore, if inorganic nanomaterials are implemented as porous nanostructures, there is an additional gain in properties associated with better adsorption capabilities and a higher number of active sites.[16] Assembly of inorganic nanomaterials into a specific configuration can also bring additional benefits. For example, multiple expansion/contraction cycles can be accommodated when yolk-shell configurations are used in rechargeable battery electrodes, whereby assuring structural integrity.[17] There is also substantial interest in synthesizing inorganic porous nanostructures within the colloidal size regime (below ~ 1 μm in at least one direction), mainly because their dynamics is controlled by thermal fluctuations (Brownian systems).[18] Self-assembling capabilities of colloids driven by thermal fluctuations complemented with some external force can generate sophisticated macrostructures at relatively low-cost in terms of simplicity.[19] Porous inorganic nanostructures with colloidal sizes seem therefore adequate for construction of efficient electrochemical devices that operate on renewable energy sources.

Advances in the synthesis of porous inorganic nanostructures are considered a key step in the development of electrochemical devices fed by renewable energy sources. Synthetic routes able to produce these nanostructures with a rigorous control in size, shape and crystallinity are essential for construction of efficient and reliable electrochemical devices. For example, control over defects and nature of exposed facets is of special importance in surface-related processes.[20] As stated above band gaps can be sensitive to minor changes in size and shape.[14] In Li-ion batteries, some systems works better at an intermediate size because a proper balance must be established between electrolyte degradation and Li diffusion.[21] In photoelectrochemical water splitting there is a size below which a semiconductor cannot longer sustain a space charge region (depletion layer).[13] The local electrostatic field within this space charge no longer separates the electron-hole pairs. Therefore, for some systems the best of the efficiencies are reached at an intermediate size. Among different synthetic routes, there is substantial experimental evidence that nowadays liquid-phase routes lead to nanostructures with a better control in size, shape and configuration.[22,23]

All previous arguments point to the importance of reports that deal with the synthesis in liquid-phase of inorganic porous nanostructures with colloidal dimensions and applicability in electrochemical energy devices. This review, thus deals with this topic. The review is organized in three main sections according to topological differences between three selected configurations (hollow, non-hollow and yolk-shell). We understand these configurations clearly show the progress made during the last years in the use of nanostructures to build

more efficient electrochemical devices. Each section has a general introduction and several subsections. In each of these subsections, we develop a topic upon what we understand is a solid and illustrative example of the synthesis, and the advantages of using such a synthesis to obtain configurations that improve electrochemical performance. More specifically, we describe how hollow porous nanostructures obtained through different synthesis methods (nanoscale Kirkendall effect, galvanic replacement reactions and hard templates) can be used to produce efficient electro-catalysts for the hydrogen evolution reaction, efficient battery conversion electrodes and better pseudocapacitors. We also describe how non-hollow porous nanostructures synthesized via the polyol and soft-template processes can be used to produce electro-catalysts for methanol electro-oxidation and insertion Li-ion anodes. Finally, we describe how yolk-shell porous nanostructures synthesized via Ostwald ripening and selective core-shell strategies can be used to produce better dye-sensitized solar cells and more stable electro-catalysts.

2. Inorganic porous nanostructures with hollow interiors and colloidal dimensions

As above-mentioned the general interest in porous nanostructures comes from the good accessibility to their nanobuilding blocks. Specifically, the interest in porous nanostructures with hollow interiors comes from their capabilities to store, to accommodate some volume changes, and to reduce the loading of high cost materials. Following Archer and Lou classification for hollow structures, the synthesis of hollow nanostructures with colloidal sizes can be grouped in conventional hard templating, sacrificial templating, soft-templating and template-free methods.[24] Hard templating basically involves the coating on a template of the active material (as precursor or in its final form) by using some adequate method, and further removal of the template preserving the shell.[25,26] Sacrificial templating routes (also known as self-templating routes) involve those routes in which the template participates both as the mold and in the reaction. They include conventional and relatively new routes such as the nanoscale Kirkendall effect or galvanic replacement reactions that we better describe below.[27] They can also include etching reactions in which the material of interest is involved in the reaction. An example is the synthesis of polyhedral Cu_2O nanocages and nanoframes via selective oxidative etching (Fig. 1).[28] Briefly, polyhedral Cu_2O nanocrystals were obtained by adding a weakly reducing agent (glucose) to a solution containing a copper citrate complex and polyvinylpyrrolidone. Then, nanocages and nanoframes were obtained by exposing the colloidal suspension to air. Selective oxidation etching via dissolution of the more unstable facets is the mechanism involved in the production of nanocages and nanoframes.

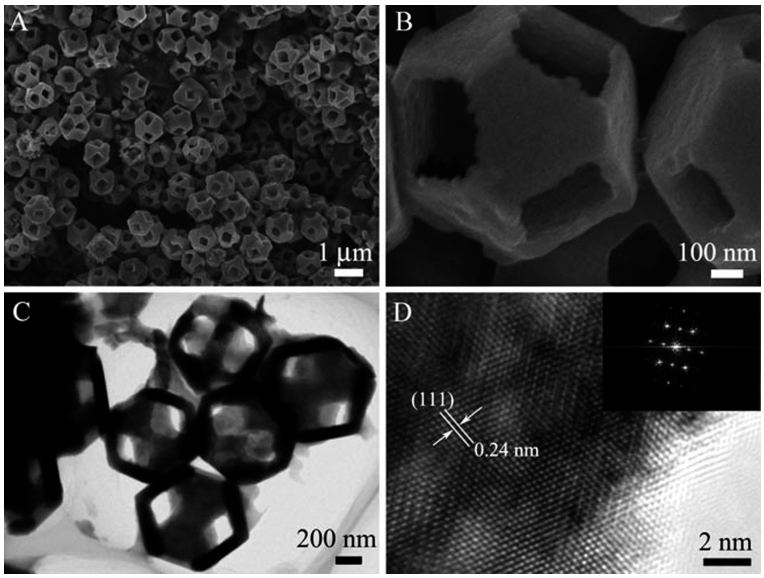

Figure 1: A) Low-magnification field-emission scanning electron microscopy (FESEM) image of Cu_2O nanoframes. B) High-magnification FESEM image of a nanoframe. C) Transmission electron microscopy (TEM) image of Cu_2O nanoframes. D) Typical High resolution TEM image of a Cu_2O nanoframe. The inset of D) shows the corresponding fast fourier transform pattern. Reproduced with permission from ref. 28, Copyright (2010) by Wiley-VCH.

Soft-templates methods are perhaps the most versatile, as they can lead to nanostructures with sizes between few nanometers to the upper limit for a colloidal system. They include emulsion droplets, supramolecular micelles, polymer aggregates/vesicles, and gas bubbles.[29] Among template-free methods, self-assembling are promising but still there are limited examples because of their inherent difficulty. Spray-pyrolysis is another template-free method that has been around for a long period of time.[30] While size control can be reached using different devices, the permeability of the shell is an issue yet to be solved in order for these routes to be competitive. Combination with other methodologies could solve this issue. For example, spray-drying techniques using polystyrene spheres as additional templates can lead to monodisperse porous nanostructures with hollow interiors and colloidal sizes.[31] Interesting monodispersity is achieved by using a cyclone connector.

2.1. The hydrogen evolution reaction with Ni_2P hollow nanostructures synthesized via the nanoscale Kirkendall effect.

Hydrogen, the third most abundant element on Earth's surface, is not available as molecular hydrogen. Therefore, it must be produced from the abundant hydrogen rich compounds through a process that consumes energy.[32] Low-cost, clean and efficient production of molecular hydrogen is thus a key step in order to reach a solid economy based on hydrogen.[33]

As above-mentioned electrochemically-assisted water splitting is considered one of the friendliest approaches to generate molecular hydrogen.[2] However, slow kinetics reduce the efficiency of this process. Therefore, when hydrogen is produced from the electrochemical reduction of water, there is a need for an electrocatalyst capable of rapidly generate a substantial amount of hydrogen at small overpotentials.[34] Platinum is considered the best metal catalyst but scarcity and high prices demand its replacement by other more abundant and less expensive electrocatalysts. MoS_2 and WS_2 are considered solid alternatives for replacement of platinum as they have high electrocatalytic activity and good stability at acidic medium.[35,36] Stability at acidic medium is important as the most effective exchange membrane-based electrolysis processes operate at acidic medium (proton exchange membranes).

The use of the nanoscale Kirkendall effect for the formation of hollow colloidal nanostructures was first reported in 2004.[37] The Kirkendall effect (formation of voids in alloys and solders) is the result of differences in diffusivities of the atoms across the interface, and supports the idea that vacancy exchange is involved in atomic diffusion. The difference in diffusivities thus leads to a flow of vacancies and the formation of voids through condensation of such vacancies.[38] For small volumes, vacancy coalescence into a single void can occur (hollow nanostructures). Specifically, the first report in 2004 described the formation of CoS, CoSe and CoO hollow nanostructures starting from stable dispersions of Co nanocrystals in o-dichlorobenzene. For CoS and CoSe a solution of sulfur/selenium dissolved also in o-dichlorobenzene was injected at 455 K, while a stream of O_2/Ar was used for the formation of CoO hollow nanostructures. As it is usually observed in sulfidation and oxidation of bulk cobalt under vapor at high temperature, outward diffusion of cobalt is the mechanism involved in the formation of hollow nanostructures (Kirkendall effect). The authors also noticed that the shell was nanostructured (permeable), and were able to prepare a yolk-shell configuration (Pt@CoO) by oxidation of Pt@Co core-shell nanocrystals. The authors proved the activity of the Pt core in the yolk-shell structure by a model reaction (hydrogenation of ethylene).

The nanoscale Kirkendall effect is usually associated with the need for elevated temperatures to speed up the diffusion of metal ions towards the surface. In Fe, Zn, Cu and Co nanoparticles, however, this effect has been observed at ambient conditions.[39] These results indicate that the nanoscale Kirkendall effect can be operative even under ambient conditions. The nanoscale Kirkendall effect usually yields high-quality hollow colloidal nanostructures (oxides, sulfides, phosphides, tellurides) in terms of crystallinity, shape and size control with

a relatively good efficiency at very small sizes.[24,27,40] These favorable capabilities explain the success of this synthetic route (see for example extensive reviews by the Archer, Lu and Yin groups).[24,27] However, as pointed out by these groups, in some reports the formation mechanism could be explained within the framework of other mechanisms. This is especially true when the reaction takes place under hydrothermal conditions in which Ostwald ripening processes are active.

In a solid work recently reported by the groups of Lewis and Schaak, faceted Ni_2P hollow nanostructures synthesized via the Kirkendall effect have been used as catalysts for the hydrogen evolution reaction.[41] Based on similarities between Ni_2P and MoS_2 and density functional theory calculations, these authors suggest that Ni_2P nanostructures with (001) exposed surfaces should be adequate to catalyze the hydrogen evolution reaction. To confirm their hypothesis, they synthesized faceted Ni_2P hollow nanostructures with (001) exposed surfaces, via the Kirkendall effect (Fig. 2). Specifically, these nanostructures were obtained from the reaction of Ni nanoparticles with the phosphorous generated via the decomposition of TOP (trioctylphospine). After deposition on titanium foil and further thermal treatment to eliminate surfactants, they checked the capabilities of Ni_2P for catalyzing the hydrogen evolution reaction as well as its stability in acid media. Polarization curves were registered for Ni_2P nanostructures deposited on titanium foil, and values were compared with Pt nanoparticles, glassy carbon and the bare titanium foil (Fig. 2). Current densities of 20 mA cm^{-2} at overpotentials of 130 mV were obtained for electrodes built using Ni_2P nanostructures. These values though higher than Pt compare well with those based on Mo-based nanoparticles (Mo is more expensive).

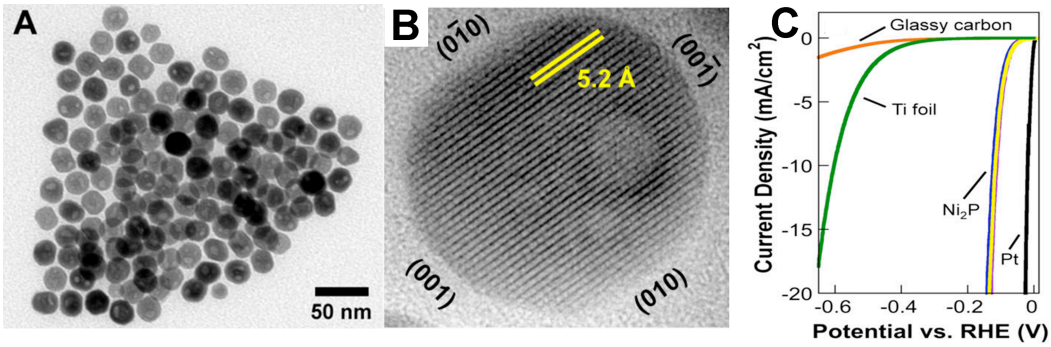

Figure 2: (A) Transmission electron microscopy (TEM) image of Ni_2P nanoparticles. (B) High-resolution TEM image of a representative Ni_2P nanoparticle, highlighting the exposed $Ni_2P(001)$ facet and the 5.2-Å lattice fringes that correspond to the (010) planes. (C) Polarization data for three individual Ni_2P electrodes in 0.5 M H_2SO_4, along with glassy carbon, Ti foil, and Pt in 0.5 M H_2SO_4, for comparison. Reproduced with permission from ref. 41, Copyright (2013) by the American Chemical Society

2.2. Conversion reaction Li-ion electrodes based on ferrite hollow nanoboxes (nanocages) synthesized via galvanic replacement reactions.

The use of conversion reaction electrodes for batteries dates back to the earliest 1980s, where several authors showed the capabilities of metallic Li to reduce some transition-metal oxides and sulfides to the metallic state.[42] Poor reversibility at room temperature as in contrast to the then emerging Li intercalation technology, almost stopped the research in these electrodes despite their inherent higher capacity. For example, the theoretical specific capacity for a conversion reaction involving the environmental friendly and earth abundant α-Fe_2O_3 (hematite) is 1010 mAh g^{-1}.[43] Renewed interest in this field arose after Tarascon and co-workers showed in the year 2000 that reversibility was possible in conversion reactions involving transition-metal oxide nanoparticles.[12] The reversibility was explained in terms of the high contact area between the resulting metallic nanoparticles and Li_2O phases. This high contact allows the decomposition of the Li_2O (otherwise electrochemically inactive) when a reverse polarization is applied. Though progress has been made during the last decade, issues such as Coulombic inefficiency in the first cycle combined with large-voltage hysteresis and the strong structural changes during the charge/discharge processes yet need to be solved.[42]

Galvanic replacement is a relatively simple self-sacrificial template redox process between a metallic template and ions of a metal having higher reduction potentials.[44] The replacement, thus, involves a continuous oxidation and dissolution of the template, and the deposition of the second metal onto the surface of the template. This method was introduced by Xia group to prepare Au, Pt and Pd hollow nanostructures from Ag nanocrystals.[45] The reduction potentials of Ag^+/Ag, $AuCl_4^-/Au$, Pd^{2+}/Pd and Pt^{2+}/Pt vs. the standard hydrogen electrode are 0.80, 0.99, 0.83 and 1.20, respectively. Therefore, galvanic replacement reactions were possible when Ag nanocrystals were dispersed in aqueous solutions containing metallic salts of these elements. Using this process the authors were able to prepare hollow nanostructures preserving the shape of the original template (spherical or cubic). Since this pioneering work, numerous reports have established galvanic replacement as the method of choice when metallic hollow nanostructures with a rigorous control in size, shape, composition and even facet selectivity is required. Notice, however, that reduction potentials are strongly dependent on the reaction conditions so caution should be taken when predicting redox reactions from standard data.

The use of galvanic replacement reactions for the formation of composite oxide nanostructures starting from binary oxide templates has been proved elusive. Up to our knowledge, the first description on the preparation of nanocages by using this approach was

recently reported by Pinna, Hyeon and co-workers.[46] In particular, iron (II) perchlorate was added to a xylene suspension containing Mn_3O_4 nanocubes, further heating led to a near-total replacement of Mn ions by Fe (III) ions, whereby forming γ-Fe_2O_3 nanocages (Fig. 3). The authors also showed the formation of nanocages for Mn_3O_4/SnO_2 and Co_3O_4/SnO_2 systems. By tuning the experimental conditions, the authors were able to synthesize Mn_3O_4/γ-Fe_2O_3 nanocages with different Mn/Fe composition. These hollow nanocages were used as conversion electrodes in Li batteries after appropriate coating with carbon and thermal treatment. Carbon is routinely used in Li-ion electrodes to improve reversibility.[47,48] These nanocages in principle can better accommodate the large differences in structure between the charge and discharge phases in conversion reactions, and so along with their high contact surface area, are expected to generate anodes with high specific capacity and good cyclability. Indeed, batteries built upon a conventional arrangement can deliver high specific capacities (close to 1000 mAh g^{-1}) at a rate of 100 mA g^{-1} for at least 50 cycles.[46] These values compare reasonably well with those obtained for the best conversion reaction electrodes.[42] Furthermore, nanocages are an ideal geometry to generate densely packed macrostructures (packing of cubes). Therefore, if the free volume of these nanocages were optimized down to the value needed to accommodate charge/discharge volume changes, they could be used to build electrodes with good mechanical stability and relatively good volumetric specific capacity. The rigorous control reached by the galvanic replacement reactions seems a good starting point to optimize that free volume.

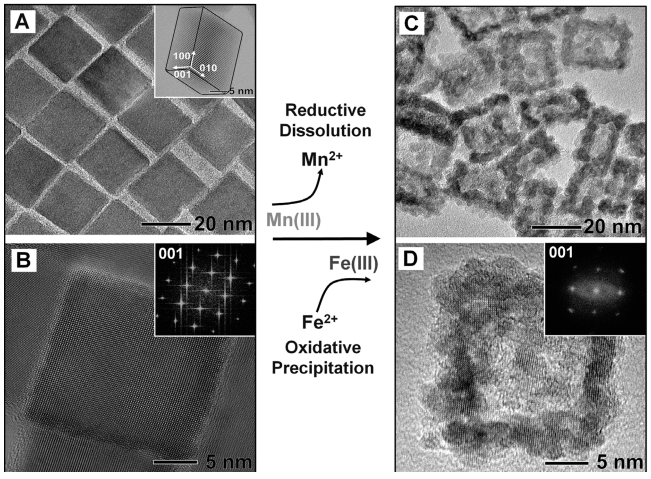

Figure 3: (A) Low-magnification transmission electron microscopy (TEM) image of Mn_3O_4 nanocrystals. The inset shows the corresponding high-resolution TEM (HRTEM) image of a single nanocrystal recorded along the [111] axis. (B) HRTEM image of a single Mn_3O_4 nanocrystal recorded along the [001] axis. The inset shows the corresponding fourier transform (FT) pattern. (C) Low-magnification TEM and (D) HRTEM images of the γ-Fe_2O_3 nanocages synthesized from the Mn_3O_4 nanocrystals**.** Reproduced with permission from ref. 46, Copyright (2013) by the American Association for the Advancement of Science (AAAS).

2.3. Pseudocapacitors based on MnO_2 hollow nanostructures synthesized via hard templating routes.

As above-mentioned electrochemical capacitors (supercapacitors) are electrochemical devices that are gaining interest because of their capacity to store/deliver energy in a short period of time. While in traditional capacitors a dielectric spacer separates two metals and charge is stored through polarization, in supercapacitors two electrodes are separated by an electrolyte and charge is stored on both electrodes.[49] Supercapacitors can store energy in the electrical double layer formed at the electrode/electrolyte interface (double-layer capacitors) or in the form of faraday reactions that take place on surfaces or close to surfaces (pseudocapacitors).[50] As surface processes are involved in charge accumulation both porosity and nanostructures are considered to be essential in any substantial improvement in efficiency at real scale. Synthesis of porous nanostructures and fundamental studies on the charge development are thus topics of interest in supercapacitors.[51-53]

The interest in supercapacitors arises from its high power density when compared to batteries. Besides, these devices can operate on the basis of long lifecycles, because the highly reversible charge storage does not involve the changes in volume and structure usually observed in secondary batteries.[54] Specifically, pseudocapacitors when compared to double-layer capacitors hold the promise of achieving higher specific energy while still retaining a high power density.[7] RuO_2 and MnO_2-based pseudocapacitors are among oxides the most promising pseudocapacitors. They have higher theoretical capacitances (800-1300 F g^{-1}) and display an ideal capacitive behavior (no significant peaks in the voltammogram and no plates in the discharge curves).[50,55] In terms of electrochemical performance, RuO_2-based electrodes are more efficient than MnO_2 electrodes, because even when built upon a conventional configuration (not as thin films) they can reach theoretical values.[56,57] However, RuO_2-based electrodes are costly and MnO_2 electrodes represent a better alternative for commercial devices. In fact MnO_2-based electrodes have long been used in commercial batteries.[58]

There is substantial evidence coming from thin films studies that high exposed surface area and good electronic contact are essential for reaching high capacitance values.[59] Therefore, a first step to improve the capacity of MnO_2 electrodes not assembled as thin films (large scale operating devices), is to synthesize nanostructures with high exposed surface area (say for example porous nanostructures with hollow interiors). As stated above hard templating methodologies can be used to prepare porous nanostructures with hollow interiors. They basically involve the coating on a solid template of the active material (as precursor or in its final form) by using some adequate method, and further removal of the solid core preserving

the shell. The origin of these methodologies is difficult to pinpoint, perhaps the seminal work by Matijevic on the preparation of monodisperse Y_2O_3 hollow spheres using monodisperse polystyrene spheres as solid templates, represents the cornerstone of this methodology.[60] Polystyrene spheres, iron oxide nanorods and specially the variety of silica templates available through synthesis are routinely used as molds. Biotemplates are also starting to gain attention as alternative molds because of the possibility to realize more complex configurations.[61] Among deposition methods, layer-by-layer and the variety of chemical deposition methods are perhaps the most employed for building hollow nanostructures.[24,62]

Hard templating methods have been used for the synthesis of MnO_2 hollow nanostructures with high surface area and good electrochemical behavior.[63] The synthesis route involved the preparation of silica spheres as templates and then the deposition of MnO_2 through a chemical solution route. Specifically, this chemical solution route consisted of a hydrothermal process at 150 °C for 48 h using $KMnO_4$ as precursor. The hydrothermal deposition generates a unique configuration that after removal of the silica template leads to hollow nanostructures with high surface area (Fig.4). Electrodes built upon a conventional configuration show ideal capacity behavior with specific values of 300 F g^{-1} (Fig.4). This value is higher than the typical values measured for other porous configurations (~200 F g^{-1}),[64] and comparable to those recently reported for similar non-doped and carbon-doped MnO_2 configurations.[65] Besides, the nanostructures show significantly good cycling stability in a neutral electrolyte (Fig. 4). These results, thus, show that hollow porous nanostructures are indeed promising for achieving better performances. Engineering nanostructures with a higher yet accessible material loading and good electronic contact could be a path to reach this goal.

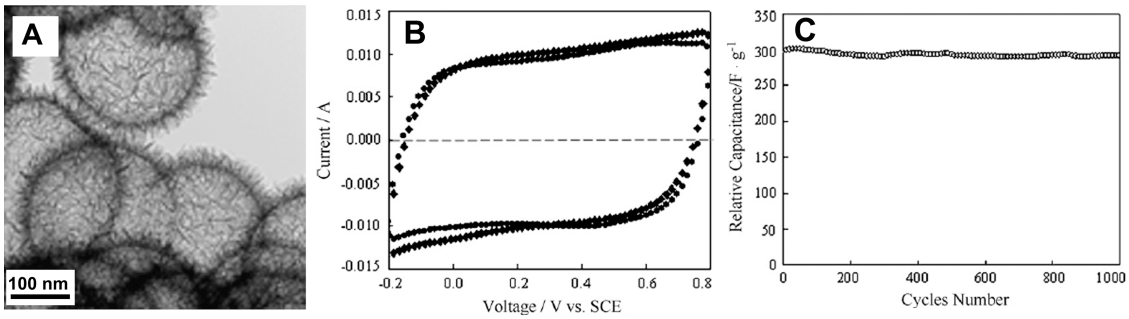

Figure 4: (A) Transmission electron microscopy image of MnO_2 hollow spheres (B) The 1st and 1000th cyclic voltammogram cycle curves at a scan rate of 5 mVs^{-1} in 1M Na_2SO_4 solution.(C) Corresponding variation of the specific capacitance with respect to cycle number between −0.2V to +0.8V vs Hg/Hg_2SO_4. Reproduced with permission from ref. 63, Copyright (2009) by Elsevier.

3. Non-hollow porous nanostructures with colloidal dimensions

A useful strategy to improve the volumetric energy and reactivity of electrochemical energy devices is to dispose of a highly accessible non-hollow porous configuration (high density of active sites). Non-hollow nanostructures with colloidal sizes can be prepared using some of the synthesis routes mentioned for hollow configurations. For example, nanocasting techniques, pioneered by the Ryoo group,[66] have been routinely used for the last 15 years (Fig. 5).[67-69] Soft-templating strategies are also the most versatile, because as stated above for the hollow configurations, they lead to nanostructures with a size from few nanometers to the upper limit for a colloidal system. Hydrothermal processes are routinely used to produce non-hollow porous nanostructures.[70] Ionic liquids can also be used to obtain uniform porous nanostructures at room temperature without using soft- or hard templates.[71] Combination of different methodologies is again a suitable route to produce this configuration. For example, spray-pyrolysis using sucrose as a sacrificial template can be used to produce non-hollow porous nanostructures of different materials.[72,73] Precursors and templates with different surface charge can be used to produce porous nanostructures by spray-drying.[31]

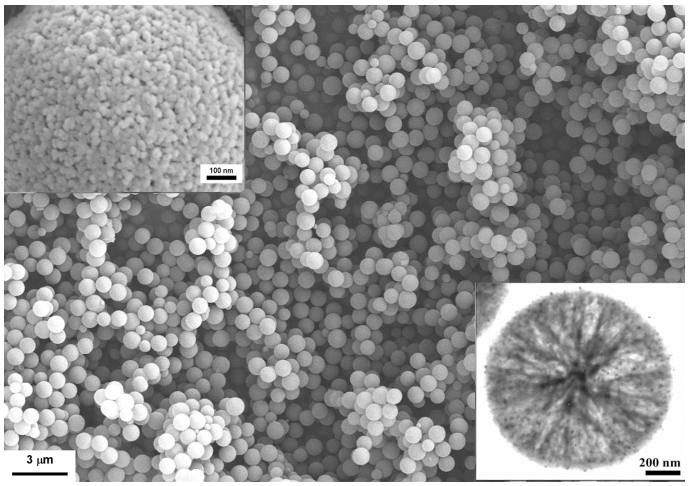

Figure 5: Field-emission scanning electron microscopy (FESEM) image of bimodal mesoporous carbon spheres MCC3b. In the upper left, high-resolution FESEM images and in the lower right transmission electron microscopy (TEM) images. We can observe in the TEM image that the large pores are aligned radially and open to the outer surface of the carbon particles. Reproduced with permission from ref. 69, Copyright (2010) by Wiley-VCH.

3.1. Methanol electro-oxidation with Pt-Cu nanodendrites synthesized via the polyol process.

Direct methanol fuel cells are a subclass of proton-exchange membrane fuel cells in which the fuel is liquid methanol.[74] These electrochemical devices are considered an alternative technology for energy supply in mobile devices because the fuel is a liquid and highly compact cells can be built. In these fuel cells, the anode reaction involves the oxidation of methanol to generate electrons that move through the external circuit, protons and CO_2. The

protons are transported through the membrane to the cathode, where they react with the O_2 and the electrons re-entering the cell through the external circuit. The product of this reaction is water. The overall reaction, thus, consists on the oxidation of methanol to generate CO_2 and H_2O. However, the methanol electro-oxidation to CO_2, which involves six electrons, is a slow process.[74] Specifically, for Pt electrodes the oxidation of adsorbed CO species is slow, and so it can be considered the rate-determining step. Pt must be alloyed with a CO-tolerant metal catalyst to enhance the efficiency for methanol oxidation.[75] There are a substantial number of Pt alloys that have been reported to achieve good electrocatalyst activity.[76] Electrocatalytic activity along with issues such as long term operating stability and Pt loading (0.2 mg cm^{-2} is the DOE target for 2015)[77] are essential to select the proper material.

The polyol process was introduced in 1989 by Fievet and co-workers as a simple solution-based method to prepare metallic particles (Ni, Co, Cu and Ag).[78] In this method a metallic precursor is solubilized/dispersed in a polyalcohol that acts both as reducing agent and solvent. The solution/suspension is stirred and heated to a temperature (the limit is the boiling point of the solvent) at which either metallic nanoparticles or intermediate oxides are formed depending on the extension of the reduction process.[79] Several polyols with different boiling points and reducing capabilities can be used in function of the material of interest. The success of this methodology mainly lays in the nature of the precursors used to produce the nanoparticles (inexpensive and easy to manipulate precursors such as hydroxides and inorganic salts).

As the abundant Cu is a relatively good catalyst for CO oxidation, Pt-Cu nanostructures seem to be an adequate alternative for efficient electrocatalysis. In fact, reports on Pt-Cu nanocubes, nanocages and nanorods show promising results at least in electrocatalytic activity.[80] Recently, a modified polyol process has been used for the synthesis of Pt-Cu nanodendrites. These nanostructures combine good accessibility with a high number of active sites and step-surface atoms (Fig.6).[81] Pt-Cu nanodendrites were synthesized through a two-step co-reduction process. Briefly, during the first step of the reaction HCl and $FeCl_3$ were injected to ethylene glycol at 110 °C. After 1 min an ethylene glycol solution containing Pt and Cu salts and polyvinylpyrrolidone was injected. The second step involved the injection of the co-reductant ascorbic acid. Therefore, during the initial step the Pt and Cu reactants are reduced by ethylene glycol in air in the presence of $FeCl_3$ and HCl. These additives together with O_2 act as oxidative etchants. Addition of ascorbic acid during the second step helps to accelerate the reduction process.

The electrocatalytic activity for methanol oxidation of the Pt-Cu nanodendrites supported on a glassy carbon substrate (Pt loading of only 0.03 mg cm^{-2}) was checked in 1M CH_3OH/0.1M $HClO_4$ solutions. The authors show that the current density at 0.9 V of the Pt-Cu nanodendrites is higher than that of Pt-Cu nanoparticles and Pt/C catalysts (Fig 6). However, stability studies show a continuous degradation in the catalytic performance of Pt-Cu nanostructures (Fig. 6), which is unequivocally associated with the dissolution of Cu. As dealloying under cell operating conditions is a general concern in Pt-based alloys,[82] it seems that in Pt-Cu nanodendrites new strategies aim to protect the alloy from dissolution while still preserving good electrocatalytic activity must be pursued. A graphitized carbon coating seems a good strategy for a better alloy protection.[83]

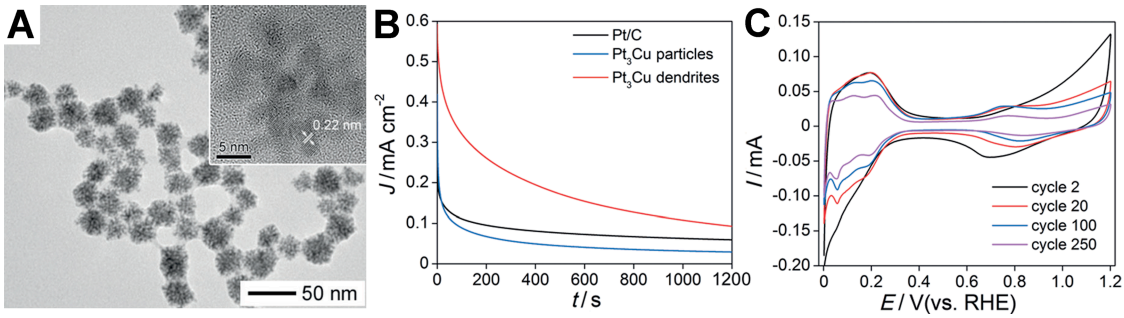

Figure 6: (A) Transmission electron microscopy (TEM) images of Pt_3Cu nanodendrites (high magnification upper right). (B) Chronoamperometry of methanol oxidation on Pt_3Cu nanodendrities, Pt_3Cu nanoparticles, and Pt/C in a solution containing 1M methanol and 0.1M $HClO_4$ at a scan rate of 50 mVs^{-1} and 0.9 V versus RHE. C) Voltammograms of Pt_3Cu nanodendrites in acid solutions. Reproduced with permission from ref. 81, Copyright (2013) by Wiley-VCH.

3.2. Insertion Li-ion anodes built upon TiO_2 porous mesocrystals synthesized via soft-templates.

TiO_2 similar to other transition-metal oxide semiconductors is considered an archetype of multifunctionality.[84] Being abundant, low cost, chemically stable and environmentally safe, it can be argued that TiO_2 along with iron oxides must be always considered as possible alternatives when commercial devices based on transition-metal oxides are fabricated. The introduction of TiO_2 as a commercial product dates back to the early 20th century, firstly as pigment and then with the use in sunscreens and toothpastes among others. Photoelectrochemical water splitting (1970s)[85] and dye-sensitized solar cells (1990s)[5] have renewed the interest in TiO_2, with new functionalities still being proposed at present. For example, TiO_2 has been used recently in efficient memristive switches (memory resistive devices that combine the electrical properties of a memory element and a resistor).[86]

Abundance, low cost, safety and chemical compatibility with the electrolyte are also the reasons for developing Li-ion batteries anodes based on titanium oxide (including lithium

titanate spinels and various TiO_2 polymorphs). These intercalation anodes with a specific capacity around 200 mAh g^{-1} operate at a relatively high voltage (~1.5V vs. Li/Li^+). Though less favorable than graphite in terms of energy density, these electrodes are safer because graphite operates at a voltage close to the Li electroplating potential (~0.1 V vs Li/Li^+).[87] Thus, TiO_2-based anodes can be a good alternative to graphite for applications in which high energy density is not required. However, performance at high rates of TiO_2-based anodes in general and more specifically of TiO_2 anatase anodes is poor. Any solid development in this figure-of-merit, thus, requires configurations in which a high number of contacts can be established.[88] Porous nanostructures with good crystallinity, accessibility and colloidal sizes below 100 nm can be promising configurations.

From oil-in-water emulsions to water-in-oil microemulsions and even spray-drying methods, the versatility of soft-template methods to produce a broad variety of porous structures has been proved in numerous reports.[89-92] Soft-template methods, thus, represents a viable alternative to produce porous nanostructures with good crystallinity, accessibility and colloidal sizes below 100 nm. Our group has recently established that conditions exist, at which the thermal destabilization of inverse microemulsions can take place through the formation of uniform self-assembled nanomicellar nanostructures with sizes below 100 nm. These soft nanostructures can act as templates for the formation of porous amorphous nanostructures.[93,94] By combining this methodology with seeded assisted chemistry, we have been able to prepare a variety of porous TiO_2 anatase mesocrystals with overall sizes below 100 nm and controlled porosity (Fig. 7).[95,96] These unique nanostructures can reach capacities of around 300 mAh g^{-1}, a value which is similar to the highest reported values.[97] Besides, these nanostructures are excellent models to check for factors that rule the electrochemical response of anodes based on anatase (Fig. 7).[96]

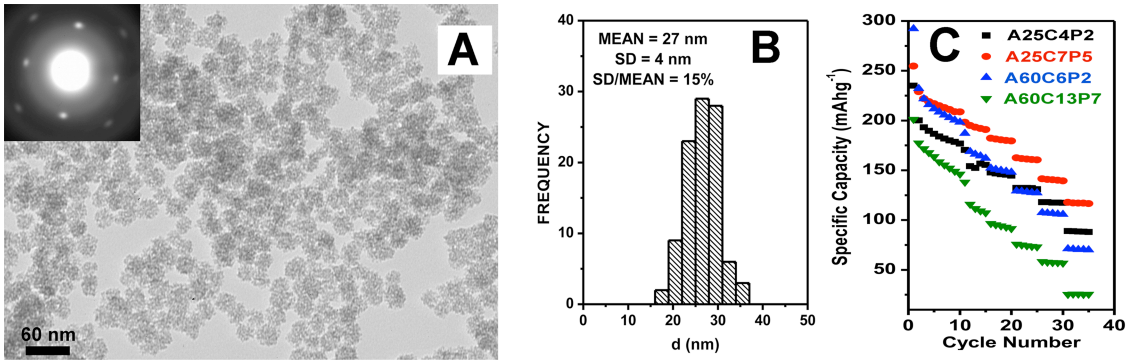

Figure 7: A) Transmission electron images of 25 nm nanostructures showing at the upper left corner a selective area electron diffraction pattern of an entire assembly, which corresponds to a single crystal. B) Histogram (% frequency units) corresponding to the transmission electron image. C) Specific capacity values for different samples cycled at different rates (0.4, 1, 2, 4, 6, and 10 C, 1 C = 0.168 A g^{-1}). A25C4P2 represents a nanostructure with an average size of 25 nanometers assembled from anatase nanocrystals of 4 nm and pores of 2 nm. In A25C7P5 the average size is also 25 nm but the nanocrystals and pores have sizes of 7 and 5 nm, respectively. In A60C6P2 and A60C13P7 the average sizes are 60 nm and the nanocrystal and pores sizes are 6 nm, 2nm and 13 nm, 7 nm, respectively. As better described in ref. 96, the best performance at high rate is obtained for the smallest nanostructure having the better accessibility (A25C7P5). Reproduced with permission from ref. 96, Copyright (2011) by Wiley-VCH.

4. Yolk-shell configurations with colloidal dimensions: Beyond hollow nanostructures

In a yolk-shell (also known as rattle-type) nanostructure, an active core is located inside the cavity of a hollow nanostructure leaving some free volume with the shell. Protection, thus, is an advantage when compared to hollow and non-hollow arrangements. Of course, the shell must have sufficient permeability to allow diffusion of reactants inside the cavity in order to reach the active core. When compared to hollow nanostructures the possibility to reach higher active material loadings is also an additional advantage of the yolk-shell configuration. However, the possibility to accommodate volume changes during operation is perhaps the fingerprint of this particular configuration. This capability is of special interest for batteries in which redox processes involve extensive volume changes. For example, Li-Si alloys are promising anodes in order to replace graphite in Li-ion batteries because they can reach a theoretical charge capacity of 4500 mAh g^{-1}. However, there is a need to accommodate volume changes of 400%. Si nanowires are so far the best configuration to accommodate such large volume changes.[98] Recently yolk-shell configurations have been introduced as a possible alternative.[17]

Broadly speaking the methodologies used to prepare these structures are based on the same concepts above-stated for the other nanostructures. Here, however, the development of the yolk-shell configuration involves different strategies.[83,99] Infiltration of hollow configurations to synthesize the active core inside the cavity is one of the strategies.[100] Other strategies are

based on the preparation of a core/shell configuration.[101] This core-shell configuration can be transformed into a yolk-shell by placing a spacer that is later dissolved. Alternatively, the transformation of the core-shell configuration can be made by taking advantage of mechanisms such as the Kirkendall effect or Ostwald ripening. In fact, as stated above in the seminal article on the application of the nanoscale Kirkendall effect to produce hollow nanostructures, the authors were able to prepare a Pt@CoO yolk-shell configuration by oxidation of Pt@Co core-shell nanocrystals, via Kirkendall effect.[37]

4.1.Dye-sensitized solar cells based on Au@TiO_2 yolk-shell nanostructures synthesized via Ostwald ripening.

In a photoelectrochemical cell, photons absorbed by a semiconductor can create electron-hole pairs that can be used either for water splitting or generation of electricity.[102] In a photosynthetic cell, the holes are involved in the oxygen formation in one electrode and electrons are involved in the hydrogen formation in the counter-electrode. These devices thus can be used to produce molecular hydrogen from water.[103,104] The electron-hole pairs can also be used to convert sunlight into electricity. Specifically, in a typical regenerative cell the negative charge carriers move to the external circuit through the semiconductor first and current collector secondly, while the positive holes are involved in the oxidation of a redox system dissolved in the electrolyte. The electrons re-entering the cell regenerate the redox system. To avoid photocorrosion while still preserving good efficiency for absorption of visible light, the Gratzel group introduced in 1991 the concept of the dye-sensitized solar cell.[5] In this device, the injection of charge carriers into stable semiconductors is achieved via visible-light photoexcitation of a dye.[5]

Strategies to increase performance in dye-sensitized solar cells focus among others in new materials such as perovskites to replace the dye itself and even the TiO_2,[105] advances in configuration (say for example scattering layers based on hollow nanostructures),[106] and doping with plasmonic metallic nanostructures.[15,107] Electrons in plasmonic metallic nanostructures can interact strongly with photons giving origin to an intense surface plasmon resonance. Specifically, this surface plasmon resonance is generated when the natural frequency of surface electrons matches that of photons. Those metallic nanostructures (for example gold metallic nanostructures) that exhibit plasmon resonance frequencies with visible photons are of particular interest for dye-sensitized solar cells. Metallic plasmonic nanoparticles under resonance conditions exhibit high absorption cross-sections (up to 10^5 larger than those of typical dye-sensitizers) together with high mobility of charge carriers.[15]

Both high absorption of photons and exceptional mobility of carriers are essential for efficient dye-sensitizers. Metallic nanostructures could thus act as dye-sensitizers. Furthermore, band-gap engineering is also possible as the plasmon resonance can be tuned with composition, size and shape.

Ostwald ripening is a well-known process that describes the growth of large particles from smaller particles basically as a result of the instability of surface atoms. Surface energy arguments, thus, predict the higher solubility of the smaller particles. Species are dissolved on the surface of the smaller particles, and when reaching adequate saturation conditions they can condense onto the surface of the more stable larger particles. Up to our knowledge this mechanism was firstly proposed in 2004 to explain the formation of TiO_2 (the anatase polymorph) hollow nanostructures of around 1 μm starting from TiF_4 solutions under hydrothermal conditions.[108] This effect has been also used in the preparation of Au@TiO_2 yolk-shell nanostructures.[109] The authors started from an Au@TiO_2 core-shell configuration. Ostwald ripening of TiO_2 component under hydrothermal conditions (180 °C) generated the yolk-shell configuration with adequate permeability in the shell. Variations of this methodology (ethanol is introduced as a co-solvent) have led to a better control in the formation of these unique nanostructures (Fig. 8).[110] This better control allows comparing the performance as photoanodes in dye-sensitized solar cells of Au@TiO_2 yolk-shell nanostructures with TiO_2 hollow nanostructures and P25 (TiO_2 from Degussa).[110] Current density-voltage curves (Fig 8) under standard AM 1.5 simulated sunlight (1000 W m^{-2}) clearly indicate an increasing performance from P25 to TiO_2 hollow and Au@TiO_2 nanostructures. The better performance of TiO_2 hollow nanostructures when compared to P25 is mainly associated with higher scattering efficiencies of the hollow spheres. The additional increase in performance when using Au@TiO_2 nanostructures is attributed to several factors all associated with the presence of Au in the nanostructure (slight decrease in open circuit voltage, the possible presence of a Schottky barrier, increases in light absorption due to surface plasmon resonances and improvements in conductivity).

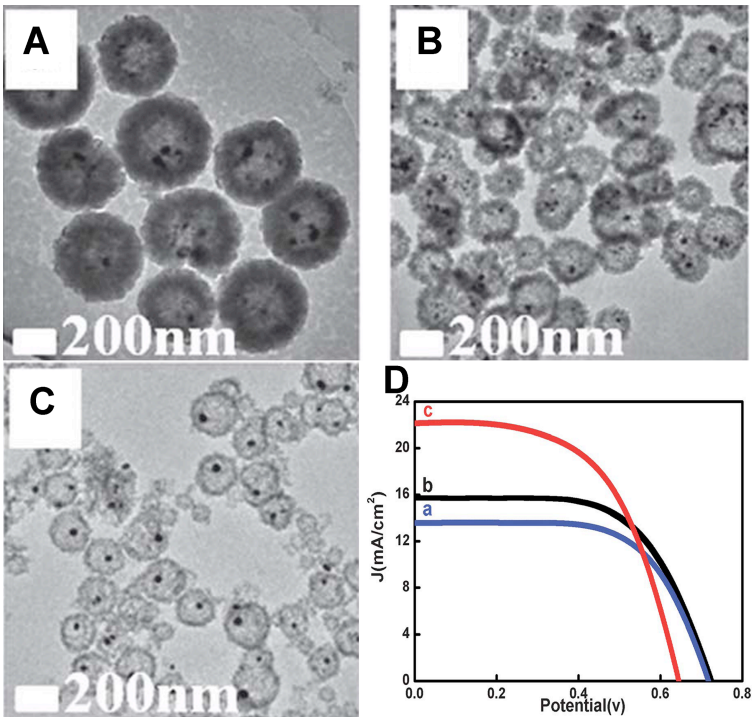

Figure 8: Transmission electron microscopy images of Au@TiO_2 hollow nanostructure with (A) thick shell, (B) medium-thickness shell, and (C) thin shell. (D) J–V curves obtained by (a) P25 (commercial TiO_2 from Degussa), (b) TiO_2 hollow nanostructures with thin shell and (c) Au@TiO_2 hollow nanostructures with thin shell. Reproduced with permission from ref. 110, Copyright (2012) by the Royal Society of Chemistry.

4.2. Electro-catalyst stability: AuPt@C yolk-shell nanostructures synthesized via a core-shell strategy.

We have already mentioned in other sections of this review the interest in using electro-catalysts for the hydrogen evolution reaction and for methanol oxidation. This interest can also be extended to the oxygen evolution reaction.[34] In any of these processes stability of the electro-catalysts is crucial for preserving the activity under operational conditions. For example, the activity of Pt or Pt-alloy nanoparticles deposited on a fuel cell cathode can be reduced by either physical processes (detachment, coalescence) or chemical processes (Ostwald ripening, dissolution or carbon support corrosion).[111] Developing configurations able to slow down these processes are thus essential for increasing the efficiency. Yolk-shell configurations seem a good starting point in order to fulfill this goal.

Schuth and Mayrhofer groups have recently reported an example in which yolk-shell nanostructures are prepared and then electrochemically tested against degradation.[83] This work is especially illustrative as the synthesis and the application can be described simultaneously. The authors prepared among others AuPt@C yolk-shell porous nanostructures. In these nanostructures, the carbon shell assures good conductivity and avoids the active core to suffer from coalescence or detachment. Furthermore, Ostwald ripening

processes are expected to slow down because the cores are relatively monodisperse. Core dissolution is expected also to slow down because high concentrations are easier to reach in the small volume in which the metal cores lay. Finally, graphitization of the nanostructures should assure better stability of the carbon shell against degradation. For the synthesis of these nanostructures the authors used the above-mentioned core-shell strategy. AuPt monodisperse colloidal solutions were firstly coated with silica and then with a combination of silica and a porogen. After heating to remove the porogen, the remaining porosity was impregnated with a carbon precursor that after a new heating protocol generated a porous carbon shell. Further treatment with NaOH removes the silica and produces a permeable yolk-shell configuration (Fig.9). Graphitization of the AuPt@C is carried out by impregnation of iron (III) nitrate followed by drying and further impregnation of the carbon precursor. To test the stability of these nanostructures against degradation the authors run a series of standard and long-term stability electrochemical tests in 0.1M $HClO_4$ solutions and find no indication of degradation during 30000 cycles.

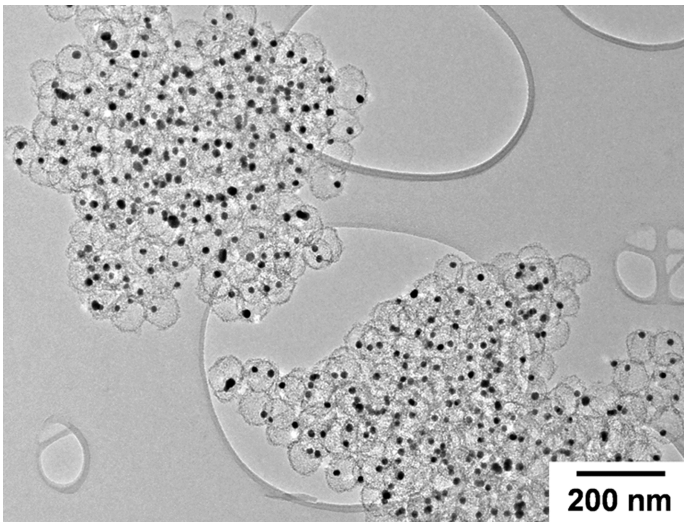

Figure 9: Transmission electron microscopy image of AuPt@C yolk-shell porous nanostructures. Reproduced with permission from ref. 83, Copyright (2013) by Wiley-VCH.

5. Perspectives and summary.

Nanoengineering at particle level can lead to even more sophisticated nanostructures to those presented in this review. Multiple quadruple-shelled hollow nanostructures can be generated by using double-shelled hollow spheres, which themselves are prepared either by partial removing of the solid core or by using single-shell hollow spheres as templates.[29] Reverse-bumpy-ball nanostructures (nanosized active materials adsorbed on the inner surface of a hollow nanostructure) can be synthesized through a multiple-step process. This process involves the use of a solid template followed by coating with seeds and a shell protecting

layer, removal of the solid core and finally growth of the seeds.[112] These hard templating methods, however, are problematic when nanostructures below about 100 nm are needed, and besides they require rigorous manipulation extended through several steps. These problems could be diminished in some alloys by combining galvanic replacement reactions with the Kirkendall effect. By using these two methods, we can have access to a variety of complex nanostructures with different size, shape and topology.[113]

Scalability, however, remains a fundamental problem to solve in order for these sophisticated nanostructures to reach the production line. Nucleation and growth are very sensitive, and scaling up processes usually lead to different configurations to those obtained under controlled lab conditions.[114] Advances in DFT (density functional theory) calculations have made possible to simulate growth processes, and so could help to solve the scalability problem.[79] Perhaps finding the right balance between sophistication, control and scalability is the best way to proceed.[115] Post synthesis routes that aim to control size via some physical principle such as centrifugation or size-exclusion chromatography also represent a good complementary tool to solve the scalability problem.

Ultimately, the landmark in the synthesis of nanostructures must be the fabrication of a device with a precise design. As mentioned in the Introduction section one of the fingerprints of colloids is their self-assembling capabilities. As devices (say for example electrodes) need to be built in order for the colloids to be functional, merely taking the colloidal nanostructure and build devices upon conventional arrangements seems to lead to a lost of efficiency. There is, thus, a need to master some of the principles that rule colloids self-assembling. The improvement in light harvesting efficiency for dye-sensitized solar cells when using photonic crystals as scattering layers, is perhaps a highly illustrative example on the importance of assembling.[116,117]

While much work has been done in self-assembling with spherical colloids, less attention has been paid to other geometries. Throughout this review, we have shown that a variety of polyhedral nanostructures can be routinely fabricated. Mastering the assembly of polyhedral nanostructures is thus of interest. However, this is an even more difficult task as reduced symmetries introduce new variables.[18] Of course, richness makes these objects more interesting as self-assembling capabilities extend well beyond those of spheres (more sophisticated nanostructures can be built). In an illustrative example recently reported, different polyhedral nanocrystals have been assembled into non-closed packed structures in solution, by taking advantage of directional entropic forces induced by depletion

interactions.[118] Alignment along their flat facets maximizes entropy, and confirms some previous theoretical work on the subject.[119]

To summarize throughout this review we have been able to demonstrate how solution techniques can produce a variety of porous nanostructures. By describing several examples we have been able to show how these nanostructures could be used as active components for more efficient electrochemical devices that operate on renewable energy sources. Yet there are some issues to solve and there is some progress to make in order for these nanostructures to reach the main market.

Acknowledgments

Financial support from projects MAT2011-23641 (to P.T.), MAT2011-25198 and MAT2011-22969 (to J.M.A.) is gratefully acknowledged.

LIST OF REFERENCES

[1] http://en.wikipedia.org/wiki/Renewable_energy#cite_note-2
[2] C. Grimes, O. K. Varghese and S. Ranjan, Light, Water, Hydrogen. (Springer, 2008)
[3] J. A. Turner, *Science*, 2013, **342**, 811-812.
[4] M. Winter and R. J. Brodd, *Chem. Rev.*, 2004, **104**, 4245-4269.
[5] B. O'Regan and M. Gratzel, *Nature*, 1991, **353**, 737-740.
[6] M. Armand and J. M. Tarascon, *Nature*, 2008, **451**, 652-657.
[7] G. Wang, L. Zhang and J. Zhang, *Chem. Soc. Rev.*, 2012, **41**, 797-828.
[8] P. Simon and Y. Gogotsi, *Nature Mat.*, 2008, **7**, 845-853.
[9] X. Cheng, C. Li, M. Gratzel, R. Kostecki and S. S. Mao, *Chem. Soc. Rev.*, 2012, **41**, 7909-7937.
[10] A. S. Arico, P. Bruce, B. Scrosati, J. M. Tarascon and W. van Schalkwijk, *Nature Mater.*, 2005, **4**, 366-377.
[11] M. Chen, C. Ye, S. Zhou and L. Wu, *Adv. Mater.*, 2013, **25**, 5343-5351.
[12] P. Poizot , S. Laruelle , S. Grugeon , L. Dupont and J. M. Tarascon , *Nature*, 2000, **407**, 496-499.
[13] A. Hagfeldt and M. Gratzel, *Chem. Rev.*, 1995, **95**, 49-68.
[14] M. A. El-Sayed, *Acc. Chem. Res.*, 2001, **34**, 257-264.
[15] S. Linic, P. Christopher and D. B. Ingram, *Nature. Mater.*, 2011, **10**, 911-921.
[16] H. Wang and A. L. Rogach, *Chem. Mater.*, DOI: 10.1021/cm4018248
[17] N. Liu, H. Wu, M. T. McDowell, Y. Yao, C. Wang and Y. Cui, *Nano Lett.*, 2012, **12**, 3315-3321.
[18] Complex Colloidal Suspensions in Soft Matter Series, Vol. 2 (Eds: G. Gompper, M. Schick), Wiley-VCH, Weinheim, Germany 2006..
[19] A. F. Demirors, P. P. Pillai, B. Kowalczyk and B. A. Grzybowski, *Nature*, 2013, **503**, 99-103.
[20] A. Fujishima, X. Zhang and D. A. Tryk, *Surf. Sci. Rep.*, 2008, **63**, 515-582.
[21] M. Aklalouch, R. M. Rojas, J. M. Rojo, I. Saadoune and J. M. Amarilla, *Electrochimica Acta*, 2009, **54**, 7542-7550.
[22] B. L. Cushing, V. L. Kolesnichenko and C. J. O'Connor, *Chem. Rev.*, 2004, **104**, 3893-3946.
[23] D. Zhang, X. Du, L. Shi and R. Gao, *Dalton Trans.*, 2012, **41**, 14455-14475; b)
[24] X. W. Lou, L. A. Archer and Z. C. Yang, *Adv. Mater.*, 2008, **20**, 3987-4019
[25] A. B. Fuertes, P. Valle-Vigon and M. Sevilla, *Chem. Commun.*, 2012, **48**, 6124-6126.
[26] N. Jayaprakash, J. Shen, S. S. Moganty, A. Corona and L. A. Archer, *Angew. Chem. Intl. Ed.*, 2011, **50**, 5904-5908.
[27] Q. Zhang, W. Wang, J. Goebl and Y. Yin, *Nanotoday*, 2009, **4**, 494-507.
[28] Y. Sui, W. Fu, Y. Zeng, H. Yang, Y. Zhang, H. Chen, Y. Li, M. Li and G. Zou, *Angew. Chem. Int. Ed.*, 2010, **49**, 4282 –4285.
[29] X. Lai, J. E. Halpert and D. Wang, *Energy Environ. Sci.*, 2012, **5**, 5604-5618.
[30] G. L. Messing, S.-C. Zhang and G. V. Jayanthi, *J. Am. Ceram. Soc.*, 1993, **76**, 2707-2726.
[31] S. Y. Lee, L. Gradon, S. Janezcko, F. Iskandar and K. Okuyama, *ACS nano*, 2010, **4**, 4717-4724.
[32] N. Armaroli and V. Balzani, *ChemSusChem*, 2011, **4**, 21-36.
[33] G. W. Crabtree, M. S. Dresselhaus and M. V. Buchanan, *Physics Today*, 2004, 57, 39-44.
[34] M. G. Walter, E. L. Warren, J. R. McKone, S. W. Boettcher, Q. Mi, E. A. Santori and N. S. Lewis, *Chem. Rev.*, 2010, **110**, 6446-6473.
[35] D. Merki and X. Hu, *Energy Environ. Sci.*, 2011, **4**, 3878-3888.
[36] J. Kibsgaard, Z. Chen, B. N. Reinecke and T. F. Jaramillo, *Nature Mater.*, 2012, **11**, 963-969.
[37] Y. Yin, R. M Rioux, C. K. Erdonmez, S. Hughes, G. A. Somorjai and A. P. Alivisatos, *Science*, 2004, **304**, 711-714.
[38] A. D. Smigelskas and E. O. Kirkendall, *Trans. AIME*, 1947, **171**, 130-142.
[39] a) C. M. Wang, D. R. Baer, L. E. Thomas, J. E. Amonette, J. Antony, Y. Qiang and G. Duscher, *J. Appl. Phys.*, 2005, **98**, 094308; b) R. Nakamura, J. G. Lee, D. Tokozakura, H. Mori and H. Nakajima, *Mater. Lett.*, 2007, **61**, 1060-1063; c) L.-I. Hung, C.-T. Wang, W. Huang and P. Yang, *Adv. Mater.*, 2010, **22**, 1910-1914; d) M. Varon, I. Ojea-Jimenez, J. Arbiol, L. Balcells, B. Martinez and V. F. Puntes, *Nanoscale*, 2013, **5**, 2429-2436.
[40] J. Lian, K. Anggara, M. Lin and Y. Chan, *Small*, DOI: 10.1002/smll.201302006.

[41] E. J. Popczun, J. R. McKone, C. G. Read, A. J. Biacchi, A. M. Wiltrout, N. S. Lewis and R. E. Schaak, *J. Am. Chem. Soc.*, 2013, **135**, 9267-9270.
[42] J. Cabana, L. Monconduit, D. Larcher and M. R. Palacin, *Adv. Mater.*, 2010, **22**, E170-E192 and *references therein*.
[43] P. Tartaj and J. M. Amarilla, *J. Power Sources*, 2011, **196**, 2164-2170.
[44] X. Xia, Y. Wang, A. Ruditskiy and Y. Xia, *Adv. Mater.*, 2013, **25**, 6313-6333.
[45] Y. Sun , B. T. Mayers and Y. Xia , *Nano Lett.*, 2002 , **2** , 481–485 .
[46] M. H. Oh, T. Yu, S.-H Yu, B. Lim, K.-T. Ko, M. G. Willinger, D.-H Seo, B. H. Kim, M. G. Cho, J.–H. Park, K. Kang, Y.-E. Sung, N.i Pinna and T. Hyeon, *Science*, 2013 , **340** , 964–968.
[47] Y. Piao, H. S. Kim, Y.-E. Sung and T. Hyeon, *Chem. Commun.*, 2010 , **46** , 118-120.
[48] C. Ban , Z. Wu , D. T. Gillaspie , L. Chen , Y. Yan , J. L. Blackburn and A. C. Dillon , *Adv. Mater.*, 2010 , **22** , E145-E149.
[49] H. Wang and H. Dai, *Chem. Soc. Rev.*, 2013, **42**, 3088-3113.
[50] B. E. Conway, *J. Electrochem. Soc.*, 1991, **138**, 1539-1548.
[51] a) T. Brezesinski, J. Wang, J. Polleux, B. Dunn and S. H. Tolbert, *J. Am. Chem. Soc.*, 2009, **131**, 1802-1809; b) Z. Chen, J. Wen, C. Yan, L. Rice, H. Sohn, M. Shen, M. Cai, B. Dunn and Y. Lu, *Adv. Energy Mater.*, 2011, **1**, 551-556.
[52] D. Carriazo, M. C. Gutierrez, F. Pico, J. M. Rojo, J. L. G. Fierro, M. L. Ferrer and F. del Monte, *ChemSusChem*, 2012, **5**, 1405-1409.
[53] W. Gu, M. Sevilla, A. Magasinsky, A. B. Fuertes and G. Yushin, *Energy Environ. Sci.*, 2013, **6**, 2465-2476.
[54] J. R. Miller and P. Simon, *Science*, 2008, **321**, 651-652.
[55] M. Toupin, T. Brousse and D. Belanger, *Chem. Mater.*, 2004, **16**, 3184-3190.
[56] F. Pico, E. Morales, J. A. Fernandez, T. A. Centeno, J. Ibañez, J., R. M. Rojas, J. M. Amarilla and J. M. Rojo, *Electrochim. Acta*, 2009, **54**, 2239-2245.
[57] X. Wu, Y. Zeng, H. Gao, J. Su, J. Liu and Z. Zhou, *J. Mater. Chem. A*, 2013, **1**, 469-472.
[58] J. M. Amarilla, F. Tedjar and C. Poinsignon, *Electrochim. Acta*, 1994, **39**, 2321-2331.
[59] X. Lang, A. Hirata, T. Fujita and M. Chen, *Nature Nanotech.*, 2011, **6**, 232-236.
[60] N. Kawahashi and E. Matijevic, *J. Colloid Interf. Sci.*, 1991, **143**, 103-110.
[61] H. Zhou, T. Fan and D. Zhang, *ChemSusChem*, 2011, **4**, 1344-1387.
[62] N. A. Dhus and K. Suslick, *J. Am. Chem. Soc.*, 2005, **127**, 2368-2369.
[63] X. Tang, Z.-H. Liu, C. Zhang, Z. Yang and Z. Wang, *J. Power Sources*, 2009, **193**, 939-943.
[64] M. Xu, L. Kong, W. Zhou and H. Li, *J. Phys. Chem. C*, 2007, **111**, 19141-19147
[65] a) S.-W. Bian, Y.-P. Zhao and C.-Y. Xian, *Mater. Lett.*, 2013,**111**, 75-77; b) Y. Zhang, M. Dong, S. Zhu, C. Liu and Z. Wen, *Mater. Res. Bull.*, 2014, **49**, 448-453.
[66] R. Ryoo, S.H. Joo and S. Jun, *J. Phys. Chem. B*, 1999, **103**, 7743-7746.
[67] A.-H. Lu and F. Schuth, *Adv. Mater.*, 2006, **18**, 1793-1805.
[68] T. Valdes-Solis and A. B. Fuertes, *Mater. Res. Bull.*, 2006, **41**, 2187-2197.
[69] A. B. Fuertes and P. Tartaj, *Small*, 2007, **3**, 275-279.
[70] Z. Wang, J. S. Chen, T. Zhu, S. Madhavi and X. W. Lou, *Chem. Commun.*, 2010, **46**, 6906-6908.
[71] D. Zhang, T. Yan, H. Li and L. Shi, *Micropor. Mesopor. Mater.*, 2011, **141**, 110-118.
[72] M. E. Fortunato, M. Rostam-Abadi and K. S. Suslick, *Chem. Mater.*, 2010, **22**, 1610-1612.
[73] Y. Xu, G. Jian, Y. Liu, Y. Zhu, M. R. Zachariah and C. Wang, *Nano Energy*, 2014, **3**, 26-35.
[74] A. S. Arico, S. Srinivasan and V. Antonucci, *Fuel Cells*, 2001, **1**, 133-161.
[75] B. C. H. Steele and A. Heinzel, *Nature*, 2001, **414**, 345-352.
[76] Z. Peng and H. Jang, *Nano Today*, 2009, **4**, 143-164.
[77] Y. Wang, K. S. Chen, J. Mishler, S. C. Cho and X. C. Adroher, *Appl. Energy*, 2011, **81**, 981-1007.
[78] F. Fievet, J. P. Lagier, B. Blin, B. Beaudoin and M. Fligarz, *Sol. State Ionics*, 1989, **32-33**, 198-205.
[79] K. J. Carrol, J. Ulises-Reveles, M. D. Shultz, S. N. Khanna and E. E Carpenter, *J. Phys. Chem. C*, 2011, **115**, 2656-2664.
[80] a) D. Xu, Z. Liu, H. Yang, Q. Liu, J. Zhang, J. Fang, S. Zou and K. Sun, *Angew. Chem. Intl. Ed.*, 2009, **48**, 4217– 4221; b) B. Y. Xia, H. B. Wu, X. Wang, X and W. Lou, *J. Am. Chem. Soc.*, 2012, **134**, 13934 –13937; c) Q. Liu, Z. Yan, N. L. Henderson, J. C. Bauer, D. W. Goodman, J. D. Batteas and R. E. Schaak, *J. Am. Chem. Soc.*, 2009, **131**, 5720– 5721.

[81] E. Taylor, S. Chen, J. Tao, L. Wu, Y. Zhu and J. Chen, *ChemSusChem*, 2013, **6**, 1863-1867.
[82] R. Borup et al., *Chem. Rev.*, 2007, **107**, 3904-3951.
[83] C. Galeano, C. Baldizzone, H. Bongard, B. Spliethoff, C. Weidenthaler, J. C. Meir, K. J. J. Mayrhofer and F. Schuth, *Adv. Funct. Mater.*, DOI: 10.1002/adfm.201302239
[84] X. Chen and S. S. Mao, *Chem. Rev.*, 2007, **107**, 2891-2959.
[85] A. Fujishima and K. Honda, *Nature*, 1972, **238**, 37–38.
[86] J. Borghetti, G. S. Snider, P. J. Kuekes, J. Joshua-Yang, D. R. Stewart and R. Stanley, *Nature*, 2010, **464**, 873-876.
[87] Y. Zhenguo, D. Choi, S. Kerisit, K.M. Rosso, D. Wang, J. Zhang, G. Graff and J. Liu, *J. Power Sources*, 2009, **192**, 588–598.
[88] Y.-G. Huo , Y.-S. Hu , W. Sigle and J. Maier , *Adv. Mater.*, 2007 , **19** , 2087-2091.
[89] C. T. Kresge, M. E. Leonowicz, W. J. Roth, J. C. Vartuli and J. S. Beck, *Nature*, 1992, **359**, 710-712.
[90] Z. Lu, M. Ye, N. Li, W. Zhong and Y. Yin, *Angew. Chem. Intl. Ed.*, 2010, **49**, 1862-1866.
[91] S. D. Sims, D. Walsh and S. Mann, *Adv. Mater.*, 1998, **10**, 151-154.
[92] M. Faustini, C. Boissiere, L. Nicole and D. Grosso, *Chem. Mater.*, DOI: 10.1021/cm402132y
[93] P. Tartaj, *Chem. Commun.*, 2009, 3228-3230.
[94] P. Tartaj, *Small*, 2010, **6** , 880-886.
[95] P. Tartaj, *Chem. Commun.*, 2011 , **47**, 256-258.
[96] P. Tartaj and J. M. Amarilla, *Adv. Mater.*, 2011 , **23**, 4904-4907.
[97] a) Y. Ren , L. J. Hardwick and P. G. Bruce , *Angew. Chem. Int. Ed.*, 2010 , **49** , 2570-2574; b) J. Wang , Y. Bai , M. Wu , J. Yin and W. F. Zhang , *J. Power Sources*, 2009 , **191** , 614-618 ; c) J. Wang , Y. Zhou , Y. Hu , R. O'Hayre and Z. Shao , *J. Phys. Chem. C*, 2011 , **115** , 2529-2536 ; d) K. Saravanan , K. Ananthanarayanan and P. Balaya , *Energy Environ. Sci.*, 2010 , **3** , 939-948.
[98] C. K. Chang, H. Peng, G. Liu, K. McIlwrath, X. F. Zhang, R. A. Huggins and Y. Cui, *Nature Nanotech.*, 2008, **3**, 31-35.
[99] M. Perez-Lozano, B. Vaz, V. Salgueiriño and M. A. Correa-Duarte, *Chem. Europ. J.*, 2013, **19**, 12196-12211.
[100] A. B. Fuertes, M. Sevilla, T. Valdes-Solis and P. Tartaj, *Chem. Mater.*, 2007, **19**, 5418-5423.
[101] R. Liu, F. Qu, Y. Guo, N. Yao and R. D. Priestley, *ChemComm*, DOI: 10.1039/c3cc47050d.
[102] M. Gratzel, *Nature*, 2001, **414**, 338-344.
[103] D. R. Gamelin, *Nature Chem.*, 2012, **4**, 965-967.
[104] M. J. Kenney, M. Gong, Y. Li, J. Z. Wu, J. Feng, M. Lanza and H. Dai, *Science*, 2013, **342**, 836-840.
[105] R. F. Service, *Science*, 2013, **342**, 794-797.
[106] C. X. He, B. X. Lei, Y. F. Wang, C. Y. Su, Y. P. Fang and D. B. Kuang, *Chem. Eur. J.*, 2010, **16**, 8757-8761.
[107] S. C. Warren and E. Thimsen, *Energy Environ. Sci.*, 2012, **5**, 5133-5146.
[108] H. G. Yang and H. C. Zeng, *J. Phys. Chem. B*, 2004, **108**, 3492-3495.
[109] J. Li and H. C. Zheng, *Angew. Chem. Intl. Ed.*, 2005, **44**, 4342-4345.
[110] J. Du, J. Qi, D. Wang and Z. Tang, *Energy Environ. Sci.*, 2012, **5**, 6914-6918.
[111] a) J. C. Meier, C. Galeano , I. Katsounaros , A. A. Topalov , A. Kostka, F. Schuth , K. J. J. Mayrhofer , *ACS Catalysis*, 2012 , **2** , 832-843; b) J. C. Meier , I. Katsounaros , C. Galeano , H. Bongard , A. A. Topalov , A. Kostka , A. Karschin , F. Schuth and K. J. J. Mayrhofer , *Energy Environ. Sci.*, 2012 , **5** , 9319-9330; c) A. A. Topalov, I. Katsounaros , M. Auinger , S. Cherevko, J. C. Meier, S. O. Klemm and K. J. J. Mayrhofer, *Angew. Chem. Intl. Ed.*, 2012, **51**, 12613-12615.
[112] M. Sanles-Sobrido, W. Exner, L. Rodriguez-Lorenzo, B. Rodriguez-Gonzalez, M. A. Correa-Duarte, R. A. Alvarez-Puebla, L. M. Liz-Marzan, *J. Am. Chem. Soc.*,2009, **131**, 2699 -2705.
[113] E. Gonzalez, J. Arbiol and V. F. Puntes, *Science*, 2011, **334**, 1377-1380.
[114] V. Sebastian, M. Arruebo and J. Santamaria, *Small*, DOI: 10.1002/smll.201301641
[115] C. M. Sim, Y. J. Hong and Y. C. Kang, *ChemSusChem*, 2013, **6**, 1320–1325
[116] S. Nishimura , N. Abrams , B. A. Lewis , L. I. Halaoui , T. E. Mallouk , K. D. Benkstein , J. van de Lagemaat and A. J. Frank, *J. Am. Chem. Soc.*, 2003, **125**, 6306 -6310.

[117] S. Colodrero, A. Mihi, J. A. Anta, M. Ocaña and H. Miguez, *J. Phys. Chem. C*, 2009, **113**, 1150-1154.
[118] K. L. Young, M. L. Personick, M. Engel, P. F. Damasceno, S. N. Barnaby, R. Bleher, T. Li, S. C. Glotzer, B. Lee and C. A. Mirkin, *Angew. Chem. Intl. Ed.*, DOI: 10.1002/anie.201306009
[119] P. F. Damasceno, M. Engel and S. C. Glotzer, *Science*, 2012, **337**,453-457.